

Dual Prompting Image Restoration with Diffusion Transformers

Dehong Kong^{1,2,*}, Fan Li^{3,*†}, Zhixin Wang³, Jiaqi Xu⁴, Renjing Pei³, Wenbo Li³, WenQi Ren^{1,2,5,†}

¹ School of Cyber Science and Technology, Shenzhen Campus of Sun Yat-sen University

²MoE Key Laboratory of Information Technology ³Huawei Noah's Ark Lab ⁴The Chinese University of Hong Kong

⁵Guangdong Provincial Key Laboratory of Information Security Technology

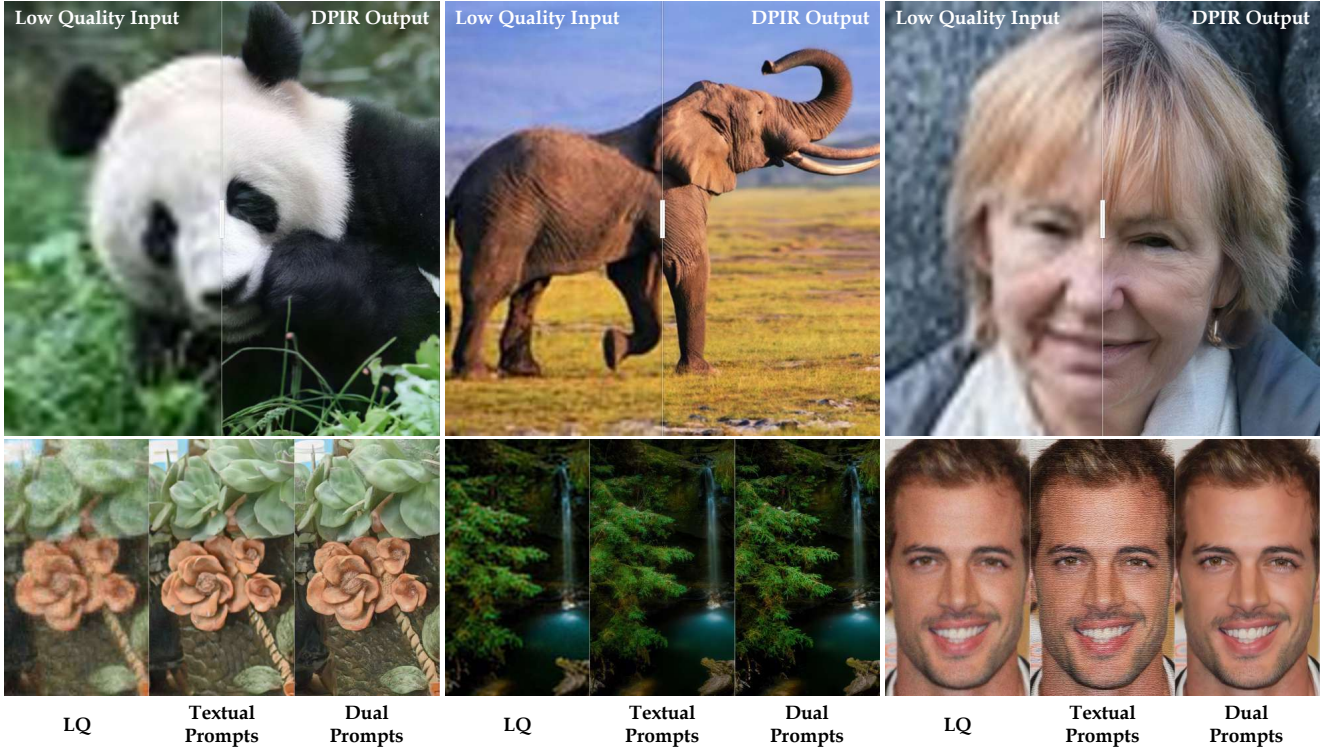


Figure 1. DPIR exhibits excellent restoration performance on real low-quality images. We compare low quality input, and the results of models using only textual prompts, and our visual-text dual prompts in the lower part. The proposed dual prompting strategy consistently outperforms the single text prompting variant in terms of image restoration quality and fidelity.

Abstract

Recent state-of-the-art image restoration methods mostly adopt latent diffusion models with U-Net backbones, yet still facing challenges in achieving high-quality restoration due to their limited capabilities. Diffusion transformers (DiTs), like SD3, are emerging as a promising alternative because of their better quality with scalability. In this paper, we introduce DPIR (Dual Prompting Image Restoration), a novel image restoration method that effectively extracts conditional information of low-quality images from multiple perspectives. Specifically, DPIR consists of two branches: a low-quality image conditioning branch and a

dual prompting control branch. The first branch utilizes a lightweight module to incorporate image priors into the DiT with high efficiency. More importantly, we believe that in image restoration, textual description alone cannot fully capture its rich visual characteristics. Therefore, a dual prompting module is designed to provide DiT with additional visual cues, capturing both global context and local appearance. The extracted global-local visual prompts as extra conditional control, alongside textual prompts to form dual prompts, greatly enhance the quality of the restoration. Extensive experimental results demonstrate that DPIR delivers superior image restoration performance.

* Contribute Equally. † Corresponding Author.

1. Introduction

The persistent demand for high-quality images across diverse fields, such as digital art and medical imaging, drives research in image restoration and super-resolution. Image restoration (IR) aims to reconstruct high-quality (HQ) images from low-quality (LQ) inputs, addressing real-world degradations of varying complexity, such as noise, blur, and compression artifacts. Recently, diffusion models-based methods [10, 42, 45, 47–49] have shown the advantages of leveraging the powerful pre-trained text-to-image (T2I) models to enhance the performance of real-world IR. These existing IR methods rely on latent diffusion models [35] with the U-Net [36] architecture, which, while effective, still encounter challenges in restoration quality. As an alternative, diffusion transformers [30] (DiTs) recently show promising generative capabilities due to their ability to capture long-range dependencies and their scalability potential, which are crucial for the quality and fidelity of restoration across a wide range of real-world situations.

Despite these advantages, effectively incorporating LQ information into DiTs remains underexplored. Existing IR methods [21, 52] based on the U-Net backbone typically utilize ControlNet [58], which incorporates the LQ image by employing a trainable copy of the U-Net’s encoding layers. In parallel, StableSR [42] adopts a lightweight trainable control network, akin to the T2I Adaptor [29], but suffers from moderate performance. However, these conditional control methods are not optimized for DiTs composed of ViT [6] blocks. This discrepancy necessitates a careful design of conditioning mechanisms for DiTs in the IR task.

In this work, we present a dual prompting image restoration model (DPIR), combined with a DiT-based diffusion model Stable Diffusion 3 (SD3) [8]. We propose several key techniques in DPIR to effectively integrate control signals from LQ images into the DiT, enabling natural and faithful image restoration. DPIR includes a low-quality image conditioning branch and a dual prompting control branch, which balances model efficiency and effectiveness. Specifically, the first branch is a lightweight module designed to efficiently inject the LQ image prior into the DiT. Inspired by ControlNeXt [31], this branch extracts conditional features of LQ images by a few of convolution layers rather than heavy backbone copies like ControlNet. Notably, the lightweight module and the DiT backbone are jointly trained to handle diverse real-world scenarios.

In IR tasks, visual cues of LQ images, including the global context information and the local texture information, are crucial for desirable image restoration. These visual signals cannot be fully captured by text descriptions alone, especially considering that the DiT backbone, without a skip-connection mechanism like U-Net, hardly keeps the information of input LQ images, which are the conditioning in text-to-image models across all DiT blocks. Hence, we

design a dual prompting restoration branch to incorporate LQ information into DiT from a more comprehensive visual perspective, leveraging the knowledge of pre-trained T2I models and complementing our lightweight conditioning branch. In detail, given a cropped patch of the LQ image, we first feed it into CLIP [33] to extract local visual features. Additionally, global visual features from the surrounding regions, rich in contextual information, are also extracted. These global-local features function as visual tokens, replacing the original CLIP text features in SD3 and serving as conditioning, alongside T5 [34] text prompts as visual-text dual prompts, for each block of DiT.

As shown in Figure 1, DPIR with the dual prompting strategy demonstrates excellent restoration performance and shows a clear advantage over the simple text prompts as DiT conditioning. Additionally, to further exploit the scalability of DiTs, we use over 20 million high-quality images as training data. Experimental results validate the effectiveness of the proposed DPIR, showing compelling image restoration performance compared to recent state-of-the-art methods and achieving impressive results across a broad range of image restoration tasks.

2. Related Work

Image Restoration. IR aims to recover high-quality, degradation-free images from degraded inputs [9, 13, 55]. Early research focus on addressing specific types of image degradation, such as denoising, deblurring, and super-resolution (SR). Since the pioneering work of SRCNN [5], numerous deep learning-based approaches [3, 14, 19, 20, 37, 54, 56, 59, 60], have been developed. Recently, generative model-based IR methods are evolving, including GAN-based and diffusion-based methods, to tackle real-world IR tasks involving blind and complex degradations. DA-CLIP [27] transfers pretrained vision-language models to low-level vision tasks as a multi-task framework for image restoration.

GAN-based IR. The application of GANs for IR or SR dates back to SRGAN [18], where image degradation is modeled using bicubic downsampling. Subsequently, BSRGAN [57] and Real-ESRGAN [43] show that IR GANs can handle more complex image degradations by synthesizing more realistic HQ-LQ pairs, showing convincing results in real-world IR.

Diffusion-based IR. Early diffusion-based works [15, 16, 44] use pre-trained diffusion models [4, 12, 39] to tackle the IR problem with simple degradation modeling. Recent approaches [21, 26, 42, 48, 51, 52] use advanced pre-trained T2I models, such as Stable Diffusion [35], for real-world image restoration. These methods typically introduce adapters to incorporate LQ images as control signals into diffusion models to reconstruct HQ images. Sta-

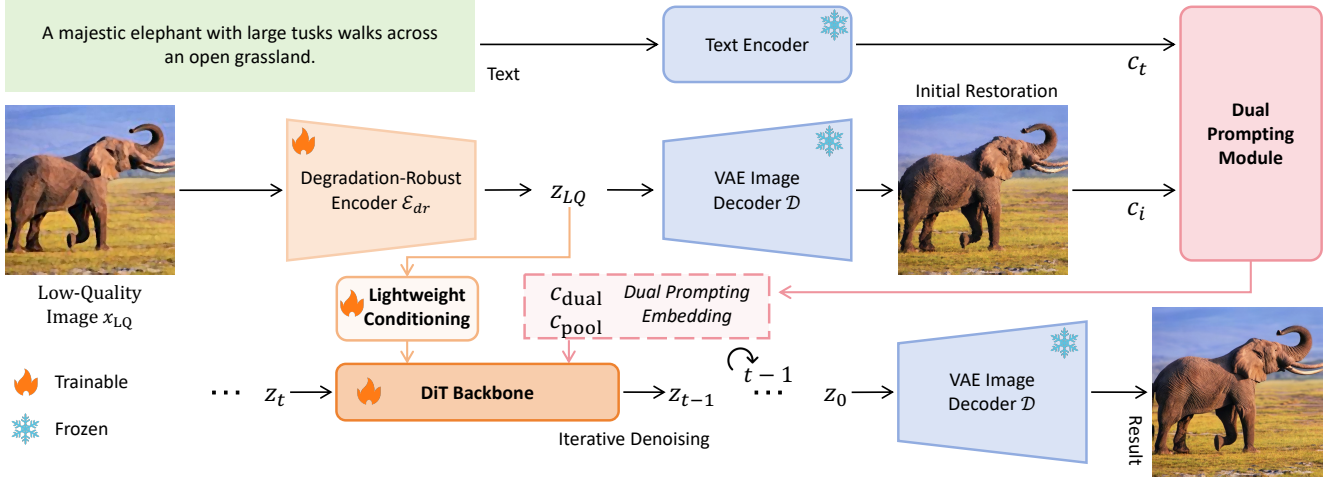


Figure 2. Framework of our proposed DPIR. Given a low-quality (LQ) image, a lightweight conditioning branch efficiently introduces the LQ information into the DiT backbone. Additionally, a dual prompting restoration branch extracts global and local visual information, alongside text prompts, to form visual-text dual prompts, which greatly enhances the restoration quality and fidelity.

bleSR [42] redesigns a time-aware encoder with LQ embedding. SUPIR [52] capitalizes on the generative capability of SDXL [32] and the captioning strength of LLaVA [23] to synthesize rich image details. In parallel, other works [45, 53] formulate customized restoration diffusion models to tackle IR, but they still exhibit suboptimal performance.

Conditional Control. Adding spatial conditional control allows powerful T2I models to generate images that follow the appearance or structures of the input reference images. ControlNet [58] proposes to use trainable copies and zero convolution to introduce conditioning. T2I-Adapter [29] instead leverages a simple and lightweight convolutional network for the controlling. ControlNeXt [31] designs an efficient control architecture and cross-normalization to facilitate training efficiency. These works target general conditional signals, such as edge, pose, or depth. In this work, we focus on designing effective conditional control methods for image restoration requiring high quality and fidelity.

3. Preliminaries

Diffusion and Flow. Diffusion models [11, 38, 40] assume a forward noising process following a specific Markov chain. We relax this and consider general generative modeling that defines a mapping [8] between samples from a noise distribution π_1 to samples x_0 from a data distribution π_0 . The forward process p_t between two distributions can be expressed as $z_t = a_t x_0 + b_t \epsilon$, where $\epsilon \sim \mathcal{N}(\mathbf{0}, \mathbf{I})$.

Recent studies, including Stable Diffusion 3 (SD3) [8], show that flow matching [22] or rectified flow [24] formulation exhibits superior performance compared to previously established diffusion formulations, particularly in high-resolution image synthesis. We follow the same rectified flow formulation, which defines a straight path be-

tween the noise distribution and the data distribution: $z_t = (1-t)x_0 + t\epsilon$. During training, we optimize the network v_θ with the conditional flow matching objective:

$$\mathcal{L}_{CFM} = \mathbb{E}_{t, p_t(z|\epsilon), p(\epsilon)} [\|v_\theta(z_t, t) - (\epsilon - x_0)\|^2] \quad (1)$$

Note that v_θ can take additional inputs besides z_t, t , such as text or other control signals.

Diffusion Transformers (DiTs). Earlier, latent diffusion models (LDMs) [32, 35] for image generation adopt the U-Net backbone, while diffusion transformers [30], which replace the U-Net backbone [36] with vision transformers (ViTs) [6], are becoming an increasing trend. DiTs show that ViT can serve as scalable architectures for diffusion models with respect to the network complexity vs. sample quality. SD3¹ [8] is a Multimodal Diffusion Transformer (MMDiT) text-to-image model that features greatly improved performance in image quality and resource efficiency, achieved through extensive training on high-quality aesthetic images. In this work, we propose to explore the power of SD3 to further advance image restoration.

4. Method

In this work, we propose DPIR, a novel image restoration model based on SD3, which consists of a low-quality image conditioning branch and a dual prompting restoration branch. Figure 2 shows the pipeline of DPIR.

4.1. Overview of DPIR

As shown in Figure 2, the input low-quality image x_{LQ} is first fed to the degradation-robust VAE encoder \mathcal{E}_{dr} to obtain the LQ image condition z_{LQ} (Sec. 4.2). Then, z_{LQ} is incorporated into the DiT via a lightweight low-quality image

¹<https://huggingface.co/stabilityai/stable-diffusion-3-medium>

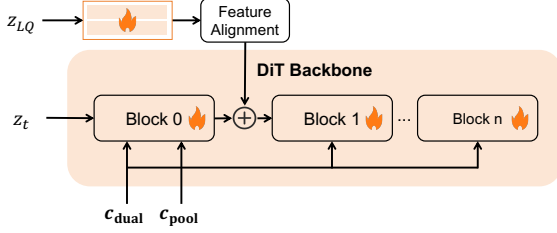


Figure 3. The LQ conditioning branch has a lightweight feature extraction module and an adaptive feature alignment module.

conditioning branch (Sec. 4.3). In parallel, z_{LQ} is mapped back to the pixel space using the VAE decoder \mathcal{D} , which together with the given textual prompts, are sent to another branch, *i.e.*, the dual prompting module, to obtain the dual prompting embeddings (Sec. 4.4). The conditional signals from these two branches guide the DiT to generate z_0 , the latents of HQ images, through iterative denoising. Moreover, we propose a global-local visual prompting training strategy to improve the restoration learning (Sec. 4.4). The learnable parameters, including the lightweight module of the LQ image conditioning branch, MLP layers of the dual prompting branch, and all DiT blocks, are jointly trained using the conditional flow matching objective, which is capable to exploit the scalability of DiTs.

4.2. Degredation-Robust VAE Encoder

We fine-tune the VAE encoder of SD3 to make our latent LQ condition, z_{LQ} , more robust to degradation, inspired by SUPIR [52]. Unlike SUPIR, we add LPIPS and GAN losses to prevent the VAE from producing overly smooth results, thereby preserving details for input images with relatively high quality. Note that the SD3 VAE with 16 latent channels outperforms SDXL VAE [32] with 4 channels, providing a better initial LQ condition for our DiT. The fine-tuning of \mathcal{E}_{dr} optimizes the following loss:

$$\|\mathcal{D}(\mathcal{E}_{dr}(x_{LQ})) - x_{HQ}\|_1 + \alpha \mathcal{L}_{lips} + \beta \mathcal{L}_{GAN}, \quad (2)$$

where α and β are weighting hyperparameters, and x_{GT} is the ground truth HQ image.

4.3. Low-Quality Image Conditioning Branch

The low-quality image conditioning branch is a lightweight module that integrates LQ conditioning z_{LQ} into the DiT backbone. The structure of this efficient image conditioning branch of DPIR is illustrated in Figure 3. Inspired by the emerging controllable generation approach, ControlNeXt [31], the LQ conditioning branch consists of two main components: a lightweight feature extraction module with a few trainable convolutional layers $\mathcal{F}_c(\cdot; \phi_c)$, and an adaptive feature alignment module η . The conditional control is incorporated into DiT with parameters θ_d by encoding the LQ features, normalizing the encoded features, and adding them to the output of DiT’s first block with parameters θ_{d_0}

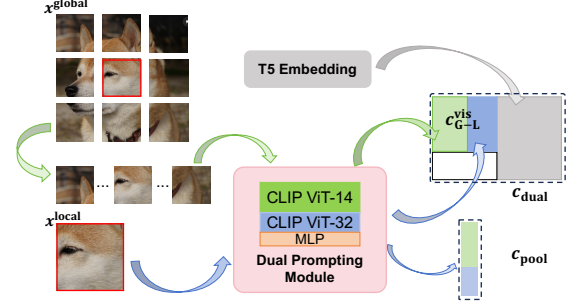


Figure 4. This figure shows a dual prompting control branch and the generation of dual embedding and cls embedding.

as follow:

$$y_c = \mathcal{F}_{d_0}(z_t; \theta_{d_0}) + \eta(\mathcal{F}_c(z_{LQ}; \phi_c); \mu, \sigma), \quad (3)$$

where $\theta_{d_0} \subseteq \theta_d, \phi_c \ll \theta_d$, z_t denotes the noisy latent at timestep t , and μ and σ are the measured mean and variance of the output features from DiT’s first block $\mathcal{F}_{d_0}(z_t; \theta_{d_0})$.

The adaptive feature alignment function η aligns the conditional features with the main branch features of DiT in terms of mean and variance, normalizing them to ensure stable and effective training.

4.4. Dual Prompting Control Branch

SD3 excels in high-quality image synthesis due to its strong multimodal language understanding, enabled by rich text embeddings and text-image cross-attention [8]. In detail, SD3 includes three types of text encoders: two CLIP [33] encoders and one T5 [34] encoder, with the final textual embeddings formed by concatenating the token embeddings of these three encoders. Additionally, the pooled embedding from the two CLIP text encoders, which captures global semantics, is also incorporated into DiT.

Inspired by the hybrid textual embeddings of SD3, we design a dual prompting module that effectively exploits the local and global visual understanding perspective from the input low-quality image, along with the textual prompt input, as illustrated in Figure 4.

4.4.1. Dual Prompting Visual Control

In image restoration, the low-quality image, x_{LQ} , serves as a crucial prior for restoring its high-fidelity image. Visual details, such as structures and textures, are difficult to be accurately described using text. Moreover, DiT lacks the skip connections in U-Net, so the lightweight LQ image conditioning in Sec. 4.3 alone is not sufficient to preserve LQ image features. To address this, we incorporate more visual control by replacing the CLIP text embeddings in DiT, which guides the restoration process more effectively.

Given a LQ image to be restored, specifically x_{LQ}^{local} for a local image patch during training, we extract its visual features using CLIP image encoders as conditional control.



Figure 5. Qualitative comparisons of different IR methods on DIV2K dataset. Our DPIR achieves the best visual performance.

For simplicity, in the following, we omit the LQ subscript from x_{LQ}^{local} , referring to it as x^{local} . In detail, we feed x^{local} into two CLIP image encoders^{2 3} to obtain their visual class token embeddings as the pooled embeddings c_{pool} , and also into the first CLIP image encoder to extract its hidden states as the visual embeddings, c_{local}^{vis} . These two visual prompt features capture the visual information of the LQ image patch from different receptive fields, replacing the original CLIP text embeddings in DiT.

4.4.2. Global-Local Visual Training

Image restoration often requires high-resolution outputs, such as 2K or 4K. Local image patches in such large images, such as only the local view of a dog’s eye, may not reveal the object or overall context of the image to be restored. This contrasts with the text control signals in pre-trained T2I models, where text captures more global semantics, which potentially leads to learning difficulties during training and reduced final performance. To address this gap, we propose a global-local visual understanding train-

ing strategy to smoothly adapt pre-trained DiT from image synthesis to image restoration.

As shown in Figure 4, during training, given a high-resolution image, we crop additional global context patches, x^{global} , surrounding the local patch x^{local} to be restored. These global patches are also fed into the first CLIP image encoder to produce the global visual features c_{global}^{vis} . These global visual tokens capture more contextual and semantic information from the input image, making them more similar to the representations of the original text embeddings in SD3. Then, we concatenate c_{global}^{vis} with previously obtained local visual tokens c_{local}^{vis} to obtain the final global-local visual prompts c_{G-L}^{vis} . Next, the visual prompts, combined with the text prompts from T5, result in the dual prompt c_{dual} , which is applied to each block in DiT via cross-attention. To enhance the model’s generalization ability across different resolutions, DPIR is trained on images with a combination of resolutions (e.g., 1k, 2k, 4k). Therefore, DPIR can set x^{global} to x^{local} when the x^{global} is not large enough to be split into patches for low-resolution inference.

²<https://huggingface.co/openai/clip-vit-large-patch14>

³<https://huggingface.co/openai/clip-vit-base-patch32>

Datasets	Methods	PSNR \uparrow	SSIM \uparrow	LPIPS \downarrow	DISTS \downarrow	CLIPQA \uparrow	MUSIQ \uparrow	NIQE \downarrow	MANIQA \uparrow
DRealsr	BSRGAN	26.50	0.6917	0.6334	0.3603	0.2402	25.22	7.7990	0.2723
	Real-ESRGAN	28.05	0.7916	0.3875	0.2514	<u>0.5593</u>	58.84	5.8095	0.3883
	StableSR	28.12	0.7735	0.3634	<u>0.2270</u>	0.4812	48.81	6.2847	0.2782
	SinSR	26.83	0.6352	0.5849	<u>0.2877</u>	0.6195	56.57	7.4154	<u>0.3618</u>
	SUPIR	25.22	0.6143	0.4992	0.2613	0.5552	59.02	5.9328	0.3607
	Ours	<u>27.31</u>	<u>0.7090</u>	<u>0.3903</u>	0.1998	0.6424	62.95	5.5463	0.3880
Realsr	BSRGAN	22.03	0.3723	0.7722	0.3795	0.3951	43.58	6.0722	0.3224
	Real-ESRGAN	26.06	0.7700	<u>0.2827</u>	0.1936	0.5157	64.46	4.4546	<u>0.3879</u>
	StableSR	26.35	0.7407	0.3083	<u>0.1990</u>	<u>0.5557</u>	60.54	4.9550	0.3415
	SinSR	25.62	0.6777	0.4036	0.2384	0.6678	<u>64.25</u>	6.0367	0.4391
	SUPIR	25.20	0.6423	0.3996	0.2268	0.5223	58.68	<u>5.3074</u>	0.3570
	Ours	26.06	<u>0.7371</u>	0.2641	0.1642	0.6625	69.28	4.7744	0.4857
DIV2K-Val	BSRGAN	<u>22.40</u>	0.5352	0.7052	0.3597	0.2228	23.24	7.2941	0.2224
	Real-ESRGAN	22.62	0.6025	<u>0.3982</u>	0.2240	<u>0.5661</u>	63.90	3.9423	<u>0.3782</u>
	StableSR	22.87	0.5844	0.3925	<u>0.2085</u>	0.4974	57.28	4.5447	0.2848
	SinSR	22.10	0.5212	0.4416	0.2160	0.6919	<u>65.13</u>	5.7650	0.4178
	SUPIR	21.23	0.5075	0.4152	0.1873	0.5239	66.49	3.7168	0.3370
	Ours	21.61	<u>0.5379</u>	0.3622	0.1677	0.7416	71.94	<u>3.9847</u>	0.5330
CelebA	BSRGAN	22.97	0.3347	0.7168	0.3311	0.5384	44.43	5.7392	0.3574
	Real-ESRGAN	30.34	0.8211	<u>0.3135</u>	<u>0.1743</u>	0.5043	63.94	5.4870	0.3285
	StableSR	29.61	0.7932	0.2925	0.1618	0.6394	66.88	<u>5.1979</u>	0.3504
	SinSR	29.19	0.7465	0.3469	0.1807	0.7940	<u>71.43</u>	6.2762	0.4348
	SUPIR	27.17	0.6479	0.3929	0.1943	<u>0.7014</u>	74.57	4.9066	<u>0.4188</u>
	Ours	<u>29.58</u>	<u>0.7739</u>	0.2449	0.1302	0.7111	71.49	4.8288	0.4414

Table 1. Quantitative comparison with state-of-the-art methods on synthetic datasets. The best, second-best, and third-best results for each

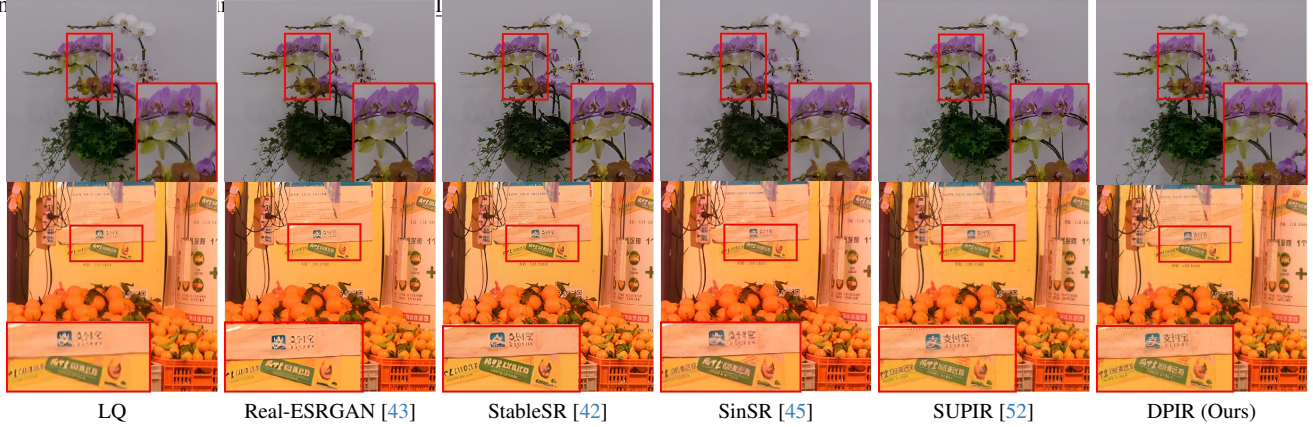


Figure 6. Qualitative comparisons of real images. DPIR delivers outstanding restoration performance, particularly in preserving details.

5. Experiments

5.1. Experimental Settings

Datasets. To meet the requirements of the base DiT, we crop images into 1024×1024 patches during training. LQ images are generated by the synthetic degradation method, following Real-ESRGAN [43]. For evaluation on synthetic data, we evaluate DPIR on DIV2K-val [1], DRealSR [46], RealSR [2] and CelebA [25]. We perform degradation

on them following [43, 52]. All datasets are cropped to 1024×1024 and degraded to 256×256 LR images. For evaluation on real-world data, we choose DRealSR and crop the HQ images to 1024×1024 for comparison purposes.

Implementation Details. For training degradation-robust VAE, we use the AdamW optimizer with a learning rate of 1×10^{-5} . We employ the same training loss as VQGAN [7], but only fine-tune the VAE encoder. During the first 5000 training steps, we use L1 loss and LPIPS [59] loss, and then

	LPIPS↓	DISTS↓	CLIPQA↑	MUSIQ↑
DACLIP-UIR	0.5686	0.3528	0.3526	47.50
DPIR (ours)	0.3903	0.1998	0.6424	62.95

Table 2. Comparison with DACLIP on DrealSR.

we use a discriminator and train for additional 20,000 steps. To train the DPIR model, including the lightweight module of the image conditioning branch, the DiT backbone, and the MLP layers of the dual prompting module, we first pre-train it on a self-collected dataset using a batch size of 1024 and a learning rate of 1×10^{-4} . Next, we fine-tune it with a batch size of 256 and a learning rate of 2×10^{-5} . This two-stage training ensures that the model benefits from a large, diverse dataset initially and further improves its detail generation performance with higher-quality data.

5.2. Comparison and Evaluation

We compare our method with several state-of-the-art methods. GAN-based methods include BSRGAN [57], Real-ESRGAN [43]. Diffusion-based methods include StableSR [42], SinSR [45], and SUPIR [52]. We adopt commonly-used no-reference metrics (*i.e.*, CLIP-IQA [41], MUSIQ [17], NIQE [28], MANIQA [50]) and reference metrics (*i.e.*, PSNR, SSIM, LPIPS, DISTS).

	PSNR↑	LPIPS↓	CLIPQA↑	MUSIQ↑
DACLIP	32.84	0.1983	0.4363	46.33
DPIR (ours)	35.46	0.1808	0.5150	57.96

Table 3. Comparison with DACLIP on PolyU.

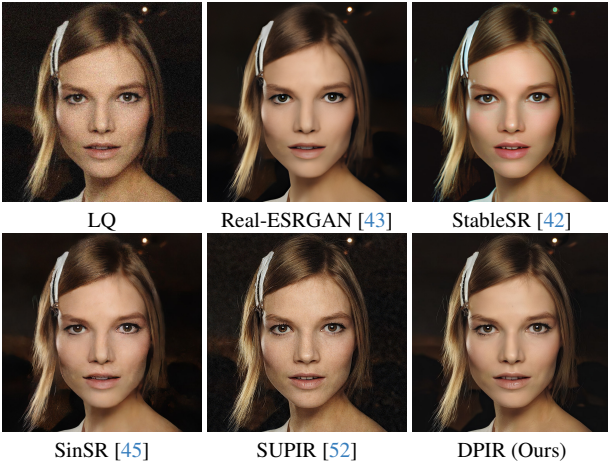


Figure 7. Qualitative comparisons on face images.

5.2.1. Evaluation on Synthetic Data

Table 1 shows the quantitative comparison results on three datasets of synthetic data. Our method consistently achieves the best or the second-best scores of DISTS, and no-reference metrics across all three datasets. In Realsr and

Methods	CLIPQA↑	MUSIQ↑	NIQE↓	MANIQA↑
BSRGAN	0.5994	62.19	3.9264	0.3555
Real-ESRGAN	0.5749	67.10	4.3671	0.4155
StableSR	0.6594	68.58	5.0153	0.4327
SinSR	0.6842	67.92	4.9608	0.4730
SUPIR	0.5632	63.93	5.2670	0.4150
Ours	0.6980	70.85	3.7382	0.5310

Table 4. Quantitative comparison with state-of-the-art methods on real-world benchmarks.

DIV2K dataset, our method has the best score of LPIPS. In particular, our method achieves a significant lead in no-reference metrics.

Figure 5 shows qualitative comparison results, illustrating the superiority of our method in terms of visual effects. Even under severe degradation, our method still maintains good fidelity and shows strong detail reconstruction capabilities. Most diffusion model-based methods struggle to maintain semantic consistency with the low-quality image, often producing incorrect textures. Our method accurately restores details in various scenes, such as the structures of animals, windows of buildings, and leaves of plants.

We also compared DPIR and DACLIP in SR and denoising tasks. Table 2 and Table 3 show our strong performance. Furthermore, to demonstrate that our method performs well on specific image categories, we validate its performance on a face dataset without any additional fine-tuning. The quantitative metrics and visual results are presented in Table 1 and Figure 7, respectively. Our method achieves excellent results in facial restoration, outperforming other approaches in both quantitative metrics and visual quality.

5.2.2. Evaluation on Real-World Data

We adopt DRealSR [46] dataset as the real-world LQ test-set. The qualitative results are shown in Table 4, and the qualitative results are shown in Figure 6. In addition to achieving the best performance across all no-reference metrics, our visual results also surpass previous methods in terms of detail and fidelity. These results demonstrate that our method performs exceptionally well on real data, effectively addressing complex real-world degradations across a wide range of scenarios. We provide more visual comparisons and a user study in the appendix.

5.3. Ablation Study

Prompting Strategy. We first discuss the significance of dual prompting in improving model performance. Specifically, we compare our dual prompting method against methods that rely solely on textual prompting or visual prompting. Textual prompting refers to the original SD3 implementation and visual prompting involves using only the extracted visual prompts from CLIP while removing T5 text prompts. As shown in Table 5, dual prompting leads to improvements in nearly all metric scores, significantly enhanc-

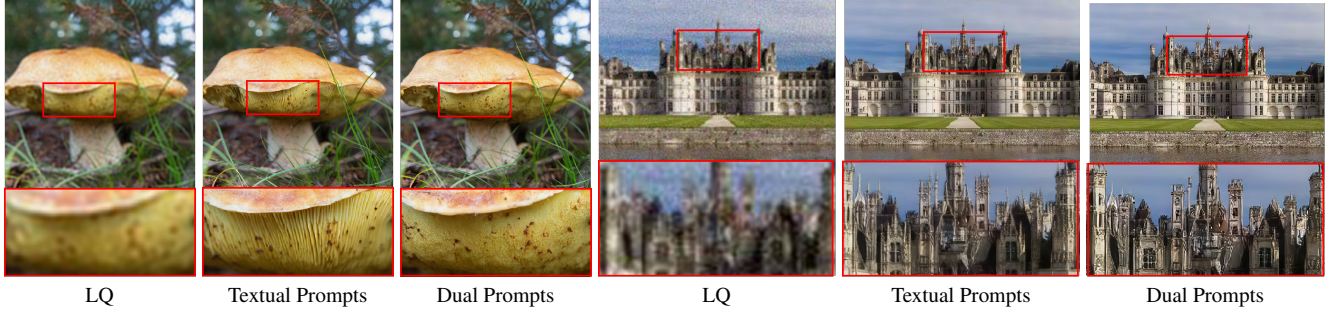


Figure 8. Qualitative comparisons of different control prompting strategies. Our dual prompting achieves the best visual results.

Methods	PSNR \uparrow	SSIM \uparrow	LPIPS \downarrow	DISTS \downarrow	CLIPQA \uparrow	MUSIQ \uparrow	NIQE \downarrow	MANIQA \uparrow
Text Prompts Only	27.21	0.7047	0.4217	0.2173	0.5614	57.08	5.7048	0.3446
Visual Prompts Only	28.69	0.7239	0.6239	0.3739	0.4106	40.97	12.6444	0.29278
Dual Prompts	27.63	0.7164	0.3846	0.1981	0.6175	60.30	5.5820	0.3650

Table 5. Quantitative comparison with Text Prompting, Image Prompting and Dual Prompting.

Methods	LPIPS	CLIPQA \uparrow	MUSIQ \uparrow	MANIQA \uparrow
Local	0.3622	0.6730	69.37	0.4315
Global-Local	0.3284	0.7416	71.94	0.5330

Table 6. Quantitative comparison of global-local and local visual



Figure 9. Visual comparisons of global-local and local methods.

ing the image restoration quality, particularly in terms of image aesthetics. Figure 8 shows the visual effectiveness of the dual prompting method across different scenarios. Note that the visual prompting variant lags largely behind text prompting (Table 5), so we primarily compare against text prompting, the default setting in SD3. We attribute this performance degradation to the absence of control signals, where text provides essential overall information about the scene or object to be restored. Overall, our dual prompting, combining visual and textual information from the low-quality image, significantly enhances restoration outcomes.

Global-Local Visual Training. We conduct ablation studies to evaluate the effectiveness of the global-local visual training strategy by performing experiments with and without extracting global-local visual features in dual prompting during training. The “Local” variant extracts visual features solely from the local input patch, while “Global-Local” also leverages the global visual context from neighboring patches. Table 6 and Figure 9 present the quantitative and qualitative results, respectively. Our

global-local visual training method greatly improve the restoration performance in terms of the image quality, substantially boosting scores across all metrics. From the visual results, the model using this training method can faithfully restore details. In contrast, the model trained using only local information tends to produce less accurate details. We attribute this to a misunderstanding of the scene to be restored, as training solely with local visual information tends to focus on generating textures rather than preserving correct overall semantics. Instead, during training, global-local visual information helps the model reduce the learning difficulty of restoring specific regions by providing context awareness.

6. Conclusion

This paper presents DPIR, a novel DiT-based image restoration method and a new dual prompting strategy that extracts valuable visual conditioning from both global and local perspectives, significantly enhancing restoration outcomes. Experimental results demonstrate DPIR’s superior performance.

Acknowledgment. This work has been supported in part by National Natural Science Foundation of China (Nos. 62322216, 62172409, 62311530686, U24B20175), research on the Optimization of Government Affairs Services (No. PBD2024-0521), research on the Detection and Analysis of Fake Threat Intelligence (No. C22600-15)

References

- [1] Eirikur Agustsson and Radu Timofte. Ntire 2017 challenge on single image super-resolution: Dataset and study. In *Proceedings of the IEEE Conference on Computer Vision and Pattern Recognition workshops*, pages 126–135, 2017. 6
- [2] Jianrui Cai, Hui Zeng, Hongwei Yong, Zisheng Cao, and Lei Zhang. Toward real-world single image super-resolution: A new benchmark and a new model. In *Proceedings of the IEEE/CVF International Conference on Computer Vision*, pages 3086–3095, 2019. 6
- [3] Xiangyu Chen, Xintao Wang, Jiantao Zhou, Yu Qiao, and Chao Dong. Activating more pixels in image super-resolution transformer. In *Proceedings of the IEEE/CVF Conference on Computer Vision and Pattern Recognition*, pages 22367–22377, 2023. 2
- [4] Prafulla Dhariwal and Alexander Nichol. Diffusion models beat gans on image synthesis. *Advances in neural information processing systems*, 34:8780–8794, 2021. 2
- [5] Chao Dong, Chen Change Loy, Kaiming He, and Xiaoou Tang. Learning a deep convolutional network for image super-resolution. In *Computer Vision–ECCV 2014: 13th European Conference, Zurich, Switzerland, September 6–12, 2014, Proceedings, Part IV 13*, pages 184–199. Springer, 2014. 2
- [6] Alexey Dosovitskiy. An image is worth 16x16 words: Transformers for image recognition at scale. *arXiv preprint arXiv:2010.11929*, 2020. 2, 3
- [7] Patrick Esser, Robin Rombach, and Björn Ommer. Taming transformers for high-resolution image synthesis. *2021 IEEE/CVF Conference on Computer Vision and Pattern Recognition (CVPR)*, pages 12868–12878, 2020. 6
- [8] Patrick Esser, Sumith Kulal, Andreas Blattmann, Rahim Entezari, Jonas Müller, Harry Saini, Yam Levi, Dominik Lorenz, Axel Sauer, Frederic Boesel, et al. Scaling rectified flow transformers for high-resolution image synthesis. In *ICML*, 2024. 2, 3, 4
- [9] Yuchen Fan, Jiahui Yu, Yiqun Mei, Yulun Zhang, Yun Fu, Ding Liu, and Thomas S Huang. Neural sparse representation for image restoration. *Advances in Neural Information Processing Systems*, 33:15394–15404, 2020. 2
- [10] Xiao He, Huaao Tang, Zhijun Tu, Junchao Zhang, Kun Cheng, Hanting Chen, Yong Guo, Mingrui Zhu, Nannan Wang, Xinbo Gao, et al. One step diffusion-based super-resolution with time-aware distillation. *arXiv preprint arXiv:2408.07476*, 2024. 2
- [11] Jonathan Ho, Ajay Jain, and Pieter Abbeel. Denoising diffusion probabilistic models. *Advances in neural information processing systems*, 33:6840–6851, 2020. 3
- [12] Jonathan Ho, Ajay Jain, and Pieter Abbeel. Denoising diffusion probabilistic models. *Advances in neural information processing systems*, 33:6840–6851, 2020. 2
- [13] Gu Jinjin, Cai Haoming, Chen Haoyu, Ye Xiaoxing, Jimmy S Ren, and Dong Chao. Pipal: a large-scale image quality assessment dataset for perceptual image restoration. In *European conference on computer vision*, pages 633–651. Springer, 2020. 2
- [14] Justin Johnson, Alexandre Alahi, and Li Fei-Fei. Perceptual losses for real-time style transfer and super-resolution. In *Computer Vision–ECCV 2016: 14th European Conference, Amsterdam, The Netherlands, October 11–14, 2016, Proceedings, Part II 14*, pages 694–711. Springer, 2016. 2
- [15] Bahjat Kavar, Gregory Vaksman, and Michael Elad. Snips: Solving noisy inverse problems stochastically. *Advances in Neural Information Processing Systems*, 34:21757–21769, 2021. 2
- [16] Bahjat Kavar, Michael Elad, Stefano Ermon, and Jiaming Song. Denoising diffusion restoration models. *Advances in Neural Information Processing Systems*, 35:23593–23606, 2022. 2
- [17] Junjie Ke, Qifei Wang, Yilin Wang, Peyman Milanfar, and Feng Yang. Musiq: Multi-scale image quality transformer. In *Proceedings of the IEEE/CVF International Conference on Computer Vision*, pages 5148–5157, 2021. 7
- [18] Christian Ledig, Lucas Theis, Ferenc Huszar, Jose Caballero, Andrew Cunningham, Alejandro Acosta, Andrew Aitken, Alykhan Tejani, Johannes Totz, Zehan Wang, et al. Photo-realistic single image super-resolution using a generative adversarial network. In *Proceedings of the IEEE Conference on Computer Vision and Pattern Recognition*, pages 4681–4690, 2017. 2
- [19] Jingyun Liang, Jie Zhang Cao, Guolei Sun, Kai Zhang, Luc Van Gool, and Radu Timofte. Swinir: Image restoration using swin transformer. In *Proceedings of the IEEE/CVF International Conference on Computer Vision*, pages 1833–1844, 2021. 2
- [20] Bee Lim, Sanghyun Son, Heewon Kim, Seungjun Nah, and Kyoung Mu Lee. Enhanced deep residual networks for single image super-resolution. In *Proceedings of the IEEE Conference on Computer Vision and Pattern Recognition workshops*, 2017. 2
- [21] Xinqi Lin, Jingwen He, Ziyang Chen, Zhaoyang Lyu, Bo Dai, Fanghua Yu, Wanli Ouyang, Yu Qiao, and Chao Dong. Diffbir: Towards blind image restoration with generative diffusion prior. *arXiv preprint arXiv:2308.15070*, 2023. 2
- [22] Yaron Lipman, Ricky TQ Chen, Heli Ben-Hamu, Maximilian Nickel, and Matt Le. Flow matching for generative modeling. *arXiv preprint arXiv:2210.02747*, 2022. 3
- [23] Haotian Liu, Chunyuan Li, Qingyang Wu, and Yong Jae Lee. Visual instruction tuning. *Advances in neural information processing systems*, 36, 2024. 3
- [24] Xingchao Liu, Chengyue Gong, and Qiang Liu. Flow straight and fast: Learning to generate and transfer data with rectified flow. *arXiv preprint arXiv:2209.03003*, 2022. 3
- [25] Ziwei Liu, Ping Luo, Xiaogang Wang, and Xiaoou Tang. Deep learning face attributes in the wild. In *Proceedings of the IEEE/CVF International Conference on Computer Vision*, pages 3730–3738, 2015. 6
- [26] Xiaobin Lu, Xiaobin Hu, Jun Luo, Ben Zhu, Yaping Ruan, and Wenqi Ren. 3d priors-guided diffusion for blind face restoration. In *Proceedings of the 32nd ACM International Conference on Multimedia*, pages 1829–1838, 2024. 2
- [27] Ziwei Luo, Fredrik K Gustafsson, Zheng Zhao, Jens Sjölund, and Thomas B Schön. Controlling vision-language

- models for multi-task image restoration. *arXiv preprint arXiv:2310.01018*, 2023. 2
- [28] Anish Mittal, Rajiv Soundararajan, and Alan C Bovik. Making a “completely blind” image quality analyzer. *IEEE Signal processing letters*, 20(3):209–212, 2012. 7
- [29] Chong Mou, Xintao Wang, Liangbin Xie, Yanze Wu, Jian Zhang, Zhongang Qi, and Ying Shan. T2i-adapter: Learning adapters to dig out more controllable ability for text-to-image diffusion models. In *AAAI*, 2024. 2, 3
- [30] William Peebles and Saining Xie. Scalable diffusion models with transformers. In *Proceedings of the IEEE/CVF International Conference on Computer Vision*, pages 4195–4205, 2023. 2, 3
- [31] Bohao Peng, Jian Wang, Yuechen Zhang, Wenbo Li, Ming-Chang Yang, and Jiaya Jia. Controlnext: Powerful and efficient control for image and video generation. *arXiv preprint arXiv:2408.06070*, 2024. 2, 3, 4
- [32] Dustin Podell, Zion English, Kyle Lacey, Andreas Blattmann, Tim Dockhorn, Jonas Müller, Joe Penna, and Robin Rombach. Sdxl: Improving latent diffusion models for high-resolution image synthesis. *arXiv preprint arXiv:2307.01952*, 2023. 3, 4
- [33] Alec Radford, Jong Wook Kim, Chris Hallacy, Aditya Ramesh, Gabriel Goh, Sandhini Agarwal, Girish Sastry, Amanda Askell, Pamela Mishkin, Jack Clark, et al. Learning transferable visual models from natural language supervision. In *ICML*, 2021. 2, 4
- [34] Colin Raffel, Noam Shazeer, Adam Roberts, Katherine Lee, Sharan Narang, Michael Matena, Yanqi Zhou, Wei Li, and Peter J Liu. Exploring the limits of transfer learning with a unified text-to-text transformer. *Journal of Machine Learning Research*, 2020. 2, 4
- [35] Robin Rombach, Andreas Blattmann, Dominik Lorenz, Patrick Esser, and Björn Ommer. High-resolution image synthesis with latent diffusion models. In *Proceedings of the IEEE/CVF Conference on Computer Vision and Pattern Recognition*, pages 10684–10695, 2022. 2, 3
- [36] Olaf Ronneberger, Philipp Fischer, and Thomas Brox. U-net: Convolutional networks for biomedical image segmentation. In *MICCAI*, 2015. 2, 3
- [37] Wenzhe Shi, Jose Caballero, Ferenc Huszár, Johannes Totz, Andrew P Aitken, Rob Bishop, Daniel Rueckert, and Zehan Wang. Real-time single image and video super-resolution using an efficient sub-pixel convolutional neural network. In *Proceedings of the IEEE/CVF Conference on Computer Vision and Pattern Recognition*, pages 1874–1883, 2016. 2
- [38] Jiaming Song, Chenlin Meng, and Stefano Ermon. Denoising diffusion implicit models. *arXiv preprint arXiv:2010.02502*, 2020. 3
- [39] Yang Song, Jascha Sohl-Dickstein, Diederik P Kingma, Abhishek Kumar, Stefano Ermon, and Ben Poole. Score-based generative modeling through stochastic differential equations. *arXiv preprint arXiv:2011.13456*, 2020. 2
- [40] Yang Song, Jascha Sohl-Dickstein, Diederik P Kingma, Abhishek Kumar, Stefano Ermon, and Ben Poole. Score-based generative modeling through stochastic differential equations. In *ICLR*, 2021. 3
- [41] Jianyi Wang, Kelvin CK Chan, and Chen Change Loy. Exploring clip for assessing the look and feel of images. In *AAAI*, 2023. 7
- [42] Jianyi Wang, Zongsheng Yue, Shangchen Zhou, Kelvin CK Chan, and Chen Change Loy. Exploiting diffusion prior for real-world image super-resolution. *IJCV*, 2024. 2, 3, 5, 6, 7
- [43] Xintao Wang, Liangbin Xie, Chao Dong, and Ying Shan. Real-esrgan: Training real-world blind super-resolution with pure synthetic data. In *Proceedings of the IEEE/CVF International Conference on Computer Vision*, pages 1905–1914, 2021. 2, 5, 6, 7
- [44] Yinhuai Wang, Jiwen Yu, and Jian Zhang. Zero-shot image restoration using denoising diffusion null-space model. *arXiv preprint arXiv:2212.00490*, 2022. 2
- [45] Yufei Wang, Wenhan Yang, Xinyuan Chen, Yaohui Wang, Lanqing Guo, Lap-Pui Chau, Ziwei Liu, Yu Qiao, Alex C Kot, and Bihan Wen. Sinsr: diffusion-based image super-resolution in a single step. In *CVPR*, 2024. 2, 3, 5, 6, 7
- [46] Pengxu Wei, Ziwei Xie, Hannan Lu, Zongyuan Zhan, Qixiang Ye, Wangmeng Zuo, and Liang Lin. Component divide-and-conquer for real-world image super-resolution. In *Computer Vision—ECCV 2020: 16th European Conference, Glasgow, UK, August 23–28, 2020, Proceedings, Part VIII 16*, pages 101–117. Springer, 2020. 6, 7
- [47] Rongyuan Wu, Lingchen Sun, Zhiyuan Ma, and Lei Zhang. One-step effective diffusion network for real-world image super-resolution. *arXiv preprint arXiv:2406.08177*, 2024. 2
- [48] Rongyuan Wu, Tao Yang, Lingchen Sun, Zhengqiang Zhang, Shuai Li, and Lei Zhang. Seesr: Towards semantics-aware real-world image super-resolution. In *Proceedings of the IEEE/CVF Conference on Computer Vision and Pattern Recognition*, pages 25456–25467, 2024. 2
- [49] Rui Xie, Ying Tai, Kai Zhang, Zhenyu Zhang, Jun Zhou, and Jian Yang. Addsr: Accelerating diffusion-based blind super-resolution with adversarial diffusion distillation. *arXiv preprint arXiv:2404.01717*, 2024. 2
- [50] Sidi Yang, Tianhe Wu, Shuwei Shi, Shanshan Lao, Yuan Gong, Mingdeng Cao, Jiahao Wang, and Yujiu Yang. Maniqa: Multi-dimension attention network for no-reference image quality assessment. In *Proceedings of the IEEE/CVF Conference on Computer Vision and Pattern Recognition*, pages 1191–1200, 2022. 7
- [51] Tao Yang, Rongyuan Wu, Peiran Ren, Xuansong Xie, and Lei Zhang. Pixel-aware stable diffusion for realistic image super-resolution and personalized stylization. *arXiv preprint arXiv:2308.14469*, 2023. 2
- [52] Fanghua Yu, Jinjin Gu, Zheyuan Li, Jinfan Hu, Xiangtao Kong, Xintao Wang, Jingwen He, Yu Qiao, and Chao Dong. Scaling up to excellence: Practicing model scaling for photo-realistic image restoration in the wild. In *Proceedings of the IEEE/CVF Conference on Computer Vision and Pattern Recognition*, pages 25669–25680, 2024. 2, 3, 4, 5, 6, 7
- [53] Zongsheng Yue, Jianyi Wang, and Chen Change Loy. Resshift: Efficient diffusion model for image super-resolution by residual shifting. *NeurIPS*, 2023. 3
- [54] Zongsheng Yue, Hongwei Yong, Qian Zhao, Lei Zhang, Deyu Meng, and Kwan-Yee K Wong. Deep variational net-

- work toward blind image restoration. *IEEE Transactions on Pattern Analysis and Machine Intelligence*, 2024. [2](#)
- [55] Jiale Zhang, Yulun Zhang, Jinjin Gu, Yongbing Zhang, Linghe Kong, and Xin Yuan. Accurate image restoration with attention retractable transformer. *arXiv preprint arXiv:2210.01427*, 2022. [2](#)
 - [56] Kai Zhang, Wangmeng Zuo, Yunjin Chen, Deyu Meng, and Lei Zhang. Beyond a gaussian denoiser: Residual learning of deep cnn for image denoising. *IEEE transactions on image processing*, 26(7):3142–3155, 2017. [2](#)
 - [57] Kai Zhang, Jingyun Liang, Luc Van Gool, and Radu Timofte. Designing a practical degradation model for deep blind image super-resolution. In *Proceedings of the IEEE/CVF International Conference on Computer Vision*, pages 4791–4800, 2021. [2](#), [7](#)
 - [58] Lvmin Zhang, Anyi Rao, and Maneesh Agrawala. Adding conditional control to text-to-image diffusion models. In *Proceedings of the IEEE/CVF International Conference on Computer Vision*, pages 3836–3847, 2023. [2](#), [3](#)
 - [59] Richard Zhang, Phillip Isola, Alexei A Efros, Eli Shechtman, and Oliver Wang. The unreasonable effectiveness of deep features as a perceptual metric. In *CVPR*, 2018. [2](#), [6](#)
 - [60] Yulun Zhang, Kunpeng Li, Kai Li, Lichen Wang, Bineng Zhong, and Yun Fu. Image super-resolution using very deep residual channel attention networks. In *European conference on computer vision*, pages 286–301. Springer, 2018. [2](#)